

Sgr B2 hard X-ray emission with *INTEGRAL* after 2009: still detectable?

Ekaterina Kuznetsova,^{1*} Roman Krivonos,¹ Alexander Lutovinov,^{1,2} Maïca Clavel³

¹Space Research Institute of the Russian Academy of Sciences, Profsoyuznaya 84/32, 117997 Moscow, Russia

²National Research University Higher School of Economics, Myasnitskaya str. 20, Moscow 101000, Russia

³Univ. Grenoble Alpes, CNRS, IPAG, F38000 Grenoble, France

Accepted XXX. Received YYY; in original form ZZZ

ABSTRACT

Molecular cloud Sgr B2 is a natural Compton mirror in the Central Molecular Zone. An observed fading of the Sgr B2 X-ray emission in continuum and Fe K_{α} 6.4 keV line indicates, as believed, a past X-ray flare activity of the supermassive black hole Sgr A*. The Sgr B2 was investigated by the *INTEGRAL* observatory at hard X-rays in 2003–2009, showing a clear decay of its hard X-ray emission. In this work, we present a long-term time evolution of the Sgr B2 hard X-ray continuum after 2009, associated with the hard X-ray source IGR J17475–2822 as observed by *INTEGRAL*. The 30–80 keV sky maps, obtained in 2009–2019, demonstrate a significant excess spatially consistent with IGR J17475–2822. The observed 2003–2019 light curve of IGR J17475–2822 is characterized by a linear decrease by a factor of ~ 2 until 2011, after which it reaches a constant level of ~ 1 mCrab. The source spectrum above 17 keV is consistent with a power-law model with $\Gamma = 1.4$ and a high-energy cut-off at ~ 43 keV. The Sgr B2 residual emission after ~ 2011 shows a good correspondence with models of the X-ray emission due to the irradiation of the molecular gas by hard X-rays and low-energy cosmic ray ions. We discuss the possible origin of the residual Sgr B2 emission after 2011 within these models, including theoretically predicted multiply-scattered emission.

Key words: Galaxy: center, ISM: clouds, X-rays: individual (Sgr B2)

1 INTRODUCTION

Sgr A* is a supermassive black hole (SMBH) with a mass of $\sim 4.15 \times 10^6 M_{\odot}$ distanced from us at 8.178 kpc (Gravity Collaboration et al. 2019). At the moment, Sgr A* is in a quiescent state with an X-ray luminosity of $L_{2-10 \text{ keV}} \sim 2 \times 10^{33} \text{ ergs s}^{-1}$ in the 2–10 keV energy band, which is ten orders of magnitude fainter than its Eddington luminosity predicted by the standard thin disk accretion onto a black hole (BH) (Baganoff et al. 2003). Such emission is also significantly lower than typical luminosities of active galactic nuclei (AGN) with comparable masses. It is natural to investigate whether Sgr A* was active with bright X-ray flares in the past.

Sunyaev et al. (1993) proposed the mechanism of reflection of strong X-ray flares from a low-ionized medium. This mechanism predicts hard X-ray emission with a continuum strongly absorbed at low energies and strong fluorescent Fe K_{α} emission line at 6.4 keV with an equivalent width (EW) of about 1 keV from an X-ray reflection nebulae (Sunyaev et al. 1993; Sunyaev & Churazov 1998). Such emission is observed from the molecular clouds of the Central Molecular Zone (CMZ, see Morris & Serabyn 1996) located in the Galactic Center (GC) region. The CMZ consists of $\sim 10\%$ of all molecular matter in the Galaxy and has a radius of about 200 pc. Its X-ray continuum and Fe K_{α} emission line at 6.4 keV suggest the Compton mirror mechanism. A possible source of the strong hard X-ray emission which can produce the observed emission of the CMZ is a past flaring activity of Sgr A*. A large number of molecular clouds

located in the GC region provides a unique possibility to investigate past activity of Sgr A* (Sunyaev & Churazov 1998). A variability of the molecular clouds' X-ray emission traces the propagation of the X-ray flare front from the regions closest to SMBH Sgr A* to the large distances from it (Ponti et al. 2010).

An alternative hypothesis of the GC molecular clouds X-ray emission is excitation of neutral matter by collisions with low-energy cosmic rays (LECRs, see e.g., Dogiel et al. 2009; Dogiel et al. 2013, 2014). LECRs can reproduce an X-ray continuum emission and Fe K_{α} 6.4 keV emission line via bremsstrahlung and fluorescence mechanisms, respectively (see e.g., Tatischeff 2003; Tatischeff et al. 2012). The observed fading of the molecular clouds' X-ray emission is in contradiction with the LECR hypothesis (see e.g., Dogiel et al. 2014). However, when the front of the X-ray flare finishes its propagation, constant emission caused by LECRs may become visible. For example, Chernyshov et al. (2018) suggested a scenario of a combination of reflected emission and emission excited by subrelativistic cosmic rays for a molecular cloud of the Arches cluster complex which emission was characterized by a fading non-thermal hard X-ray continuum and fluorescent Fe K_{α} 6.4 keV line (Krivonos et al. 2014, 2017a; Clavel et al. 2014; Kuznetsova et al. 2019).

Sgr B2 is the densest (10^6 cm^{-3} in its 5 pc core) and most massive molecular cloud ($\sim 10^6 M_{\odot}$) in the CMZ. Thanks to the ASCA observatory, the Sgr B2 emission in the fluorescent Fe K_{α} line was detected and its high equivalent width (EW) was measured (Koyama et al. 1996). The Sgr B2 X-ray emission at energies above 20 keV was for the first time associated with the hard X-ray source IGR J17475–2822 (hereafter IGR1747), detected with the *INTE-*

* E-mail: eakuznetsova@cosmos.ru

GRAL observatory by [Revnitsev et al. \(2004b\)](#), who concluded that Sgr B2 could be irradiated by a hard X-ray flare from Sgr A* with a luminosity of 1.5×10^{39} erg s⁻¹ in the 2–200 keV band and characterized by a spectral power-law photon index of $\Gamma \approx 1.8$. Assuming the Sgr B2 projected distance from Sgr A* to be 100 pc, [Revnitsev et al. \(2004b\)](#) concluded that the Sgr A* flare occurred 300–400 years ago. Using *INTEGRAL* observations in 2003–2009, [Terrier et al. \(2010\)](#) obtained the light curve of Sgr B2, showing a descending trend of its hard X-ray emission. The new parallax measurement of Sgr B2 obtained by [Reid et al. \(2009\)](#) suggested that Sgr B2 is 130 pc nearer than Sgr A*. [Ponti et al. \(2010\)](#), considering the new Sgr B2 position, reported that the Sgr A* flare terminated 100 years ago. Using Monte Carlo simulations, [Walls et al. \(2016\)](#) considered two cases: uniform and Gaussian Sgr B2 density profiles. The former gave an estimate of the Sgr B2 position as being 50 pc closer to the Earth than Sgr A*, corresponding to an older flare than the estimation by [Ponti et al. \(2010\)](#), while the latter suggested the Sgr B2 position at the projected distance of 100 pc that supports the 300–400-year-old flare. *NuSTAR* observations of the Sgr B2 at energies up to 40 keV in 2013 allowed for the detection of prominent X-ray features and two compact cores in the central 90''-region, which are surrounded by diffuse emission ([Zhang et al. 2015](#)). It is inconclusive whether the Fe K α emission has reached a constant background level or is continuing to decrease. Moreover, the decreasing scenario is best explained with reflection, while a constant scenario is best described by cosmic rays.

Since 2013, there were no new investigations of the Sgr B2 emission at energies higher than 20 keV. However, the *INTEGRAL* observatory has continued its work, and a large amount of new data has been collected up to 2020. It is natural to expect that the Sgr B2 X-ray emission either continues to fade towards a non-detection level or reaches a constant level or rises due to another flare from Sgr A*. Indeed, a number of works suggest several Sgr A* flares in the past that are currently propagating in the CMZ ([Clavel et al. 2013](#); [Chernyshov et al. 2018](#); [Chuard, D. et al. 2018](#); [Terrier et al. 2018](#)).

In this work, we present the long-term evolution of the Sgr B2 hard X-ray emission obtained from the whole dataset of the *INTEGRAL* observations publicly available to date. The paper is structured as follows: Sect. 2 contains a brief overview of the *INTEGRAL* data processing and used observations. The time evolution of the Sgr B2 hard X-ray emission is presented in Sect. 4. Sect. 5 describes the Sgr B2 spectral analysis. Discussion and summary are presented in Sect. 6 and 7, respectively.

2 OBSERVATIONS AND DATA ANALYSIS

All publicly available *INTEGRAL* data from December 2002 to January 2020 were selected for this work. We used the coded-aperture telescope *IBIS* ([Ubertini et al. 2003](#)), which operates in the soft gamma-ray energy band 20 keV – 10 MeV on board the *INTEGRAL* observatory ([Winkler et al. 2003](#)). For our purposes, we utilized data from the low-energy detector layer *ISGRI* ([Lebrun et al. 2003](#)) of the *IBIS* telescope. Its spatial resolution of 12' (full width at half-maximum, FWHM) provides a possibility to detect Sgr B2 individually, which corresponds to a spatial scale of ~ 30 pc at a distance of 8.5 kpc.

We used energy calibration as implemented in the *INTEGRAL* Science Data Center 'Off-line Scientific Analysis' (OSA) software version 10 for all data, but from the beginning of the 1626 revolution, OSA11 was applied to the remaining data (see details in <https://www.isdc.unige.ch/integral/>). The *INTEGRAL*

data were reprocessed with a proprietary analysis package developed at IKI¹ (details available in [Krivonos et al. 2010, 2012](#); [Churazov et al. 2014](#)). It was optimized for the *IBIS* image deconvolution using the systematic noise suppression algorithm described in [Krivonos et al. \(2010\)](#), which was proved to be effective in a number of works (see e.g., [Krivonos et al. 2012, 2017b](#)), that is crucial for the Sgr B2 image analysis in a crowded field of the GC region. For our analysis, we used individual sky images for each *INTEGRAL* observation with a typical exposure time of 2 ks (science window or ScW). To compensate the ongoing detector degradation, all ScW sky images were renormalized using the observed count rate of the Crab nebula, measured in the nearest observation, which provides smooth calibration of the ancillary response function over the whole observation time. The typical time between the Sgr B2 and Crab observations is about 30 days. As a result, final sky mosaics are constructed from the *IBIS* ScW sky images in mCrab units. Note that the described procedure automatically corrects for the intrinsic variability of the Crab Nebula flux (for details see Sect. 2.1). For spectral analysis in this work, the diagonal energy redistribution matrix is designed to reproduce the Crab spectrum, which can be represented as $10.0 \times E^{-2.1}$ keV photons cm⁻² s⁻¹ keV⁻¹ (see, e.g. [Churazov et al. 2007](#); [Madsen et al. 2017](#)). Note that the astrophysical (cosmic-ray X-ray and Galactic ridge backgrounds) and instrumental backgrounds of the *IBIS* telescope are already subtracted as a result of the coded-mask image reconstruction algorithm, so the sky images have zero expectation value and unit variance.

We selected the 30–80 keV energy band for the analysis of the Sgr B2 long-term light curve since this band is characterized by an almost constant efficiency during more than a decade of *INTEGRAL* observations, i.e., it is not strongly affected by the ongoing detector degradation. Note that errors for all estimated parameters are given at the 90% confidence interval.

2.1 Systematic noise

Before the detailed analysis of the *IBIS* data, we checked them for presence of systematic noise in the flux determination. We used the Crab Nebula flux measured in each ScW in the following energy bands: 30–80 keV (for light curves, see the next paragraph) and 17–26, 26–38, 38–57, 57–86, 86–129 keV for the Sgr B2 spectra (see Sect. 5). The relative systematic scatter of the measured fluxes was determined by dividing the standard deviation of the Crab flux by its average value during a given spacecraft revolution (~ 3 days). In all energy bands, systematic noise was found at a level of $\sim 5 - 8\%$ over the considered time interval. The obtained level of systematic noise is comparable to the variability of the Crab Nebula flux observed at the 10% level (see, e.g. [Oh et al. 2018](#)). However, we found that in the 17–26 keV energy band, relative systematic noise was significantly increased from 7% to 20 – 30% after the ~ 1500 revolution. The obtained systematic errors were taken into account in the following analysis.

Similar to [Terrier et al. \(2010\)](#), we use the Ophiuchus cluster, located at $\sim 9^\circ$ from Sgr B2, as a reference persistent X-ray source to verify our light curve extraction procedure. Fig. 3 shows the 30 – 80 keV multi-year light curve of the Ophiuchus cluster approximated with a constant function at $F_{\text{Oph}} = 1.37 \pm 0.11$ mCrab².

¹ Space Research Institute of the Russian Academy of Sciences, Moscow, Russia

² The flux unit of 1 mCrab is equivalent to the flux of $1.07 \times$

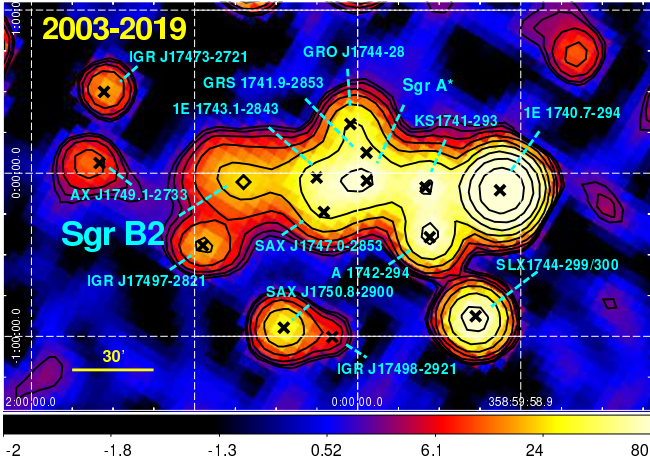


Figure 1. 2003–2019 (26–2180 *INTEGRAL* orbits) *IBIS* image of the GC region in the 30–80 keV energy band shown in detection significance units. The positions of known bright X-ray sources are marked with crosses. Solid black contours denote significance levels from 2σ to 800σ in logarithmic scale. The Sgr B2 molecular cloud is shown by a diamond.

Despite the relative weakness of the Ophiuchus cluster in the 30–80 keV band, we obtained good fit statistics characterized by a reduced chi-squared $\chi_{\text{red}}^2 = 1.4$ for 16 degrees of freedom (d.o.f.). We conclude that our *IBIS/ISGR1* light curve extraction procedure in the 30–80 keV band is not significantly affected by systematic noise related to the multi-year *ISGR1* detector degradation.

3 *IBIS/ISGR1* SKY IMAGING OF Sgr B2 REGION

We first constructed the time-averaged 30–80 keV *IBIS/ISGR1* map of the GC region using all available data from 2003 to 2020 (see Fig. 1). The *INTEGRAL* source IGR1747, spatially coincident with the position of Sgr B2 (Revnivtsev et al. 2004a; Bélanger et al. 2006), was significantly detected in the 30–80 keV band with the flux of 1.25 ± 0.04 mCrab at RA= $17^{\text{h}}47^{\text{m}}29^{\text{s}}.28$ and Dec.= $-28^{\circ}21'57''.60$ (equinox J2000). The IGR1747 centroid position is shifted by ~ 2.1 from the center of the peak of the Sgr B2 column density of the molecular gas localized between Sgr B2(N) and Sgr B2(M) cores at RA= $17^{\text{h}}47^{\text{m}}20^{\text{s}}.35$ and Dec.= $-28^{\circ}22'43''.50$ (Protheroe et al. 2008). Note that the *INTEGRAL/IBIS* point source localization accuracy depends on detection significance (Krivonos et al. 2007). Thus, the obtained offset is within the corresponding uncertainty of $\sim 3'$ (2σ) for the source detection significance of 10 – 20σ , which confirms the association of IGR1747 with the Sgr B2 molecular cloud.

The *IBIS* one-year averaged maps of the GC region shown in Fig. 2 demonstrate a clear decrease in the Sgr B2 flux from 2003 to 2009, with the corresponding drop in significance from 13σ to 4σ , which is consistent with Terrier et al. (2010) findings. On the sky maps after 2009, Sgr B2 appears as a weak source detected at a significance of $\sim 2 - 5\sigma$. Note that apparent morphology changes can not be considered real because the *INTEGRAL* localization accuracy of a weak source is $4.2'$ at the 2σ confidence interval (Krivonos et al. 2007). Also from Fig. 2, it is seen that some GC sources have strong flux variations with a timescale of less than 1 year. Contours denote a surface brightness above 2 mCrab in order to better represent of

10^{-11} erg s^{-1} cm^{-2} in the 30–80 keV energy band for a source with a spectrum similar to that of the Crab Nebula.

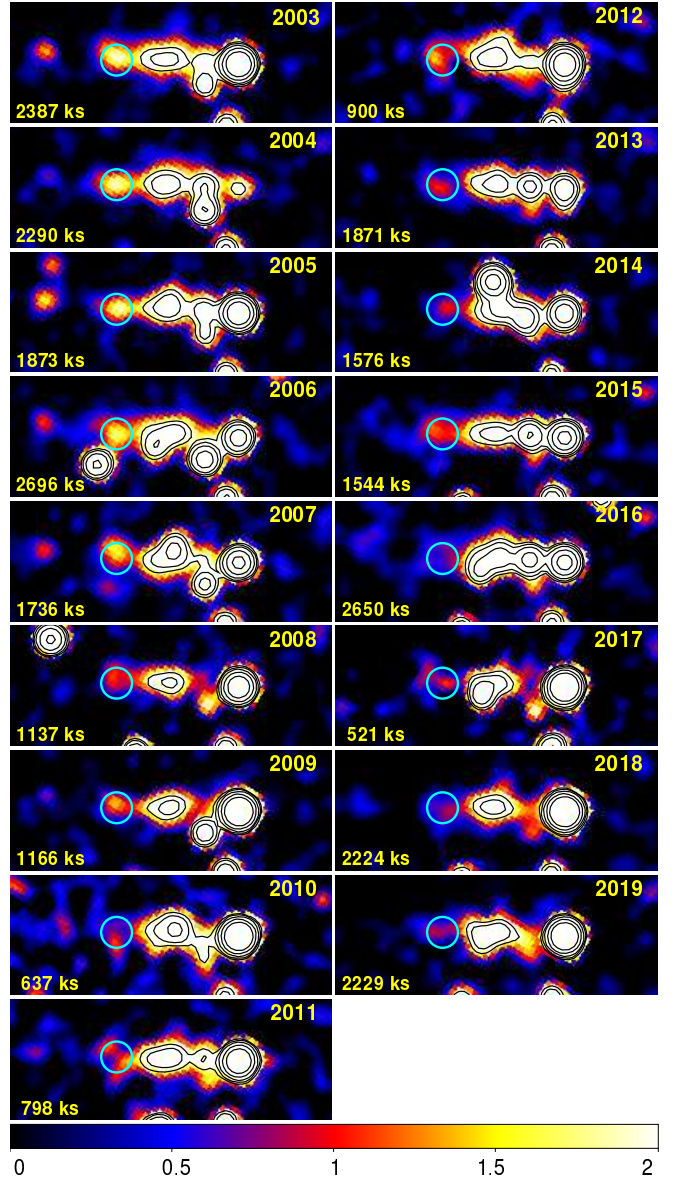


Figure 2. *IBIS* one-year averaged maps of central 4° in the 30–80 keV energy band shown in flux (mCrab units) from 2003 to 2019. Cyan circle with $R = 6'$ reveals the position of the Sgr B2 source. The corresponding years and dead-time corrected exposures are indicated in panels. Contours denote isophotes of the flux levels of 2, 3, 5, 10, and 20 mCrab.

the nearby X-ray sources with the flux higher than that of Sgr B2. Fig. 2 shows that the hard X-ray emission at the position of Sgr B2 continues to be visible after 2010.

4 LONG-TERM LIGHT CURVE OF Sgr B2

The obtained 2003–2020 *IBIS* light curve of Sgr B2 is shown in Fig. 3. The fitting procedure applied to the light curve with a simple constant function does not describe the data well enough, as reflected in the worst fit statistics $\chi_{\text{red}}^2/d.o.f. = 7.4/16$ (see Table 1), which is mainly caused by a clear decay of the Sgr B2 hard X-ray emission before 2009, as reported by Terrier et al. (2010). Therefore, the Sgr B2 flux is inconsistent with the constant function and demonstrates a few-year time variability. Note that a possible fast Sgr B2 variability,

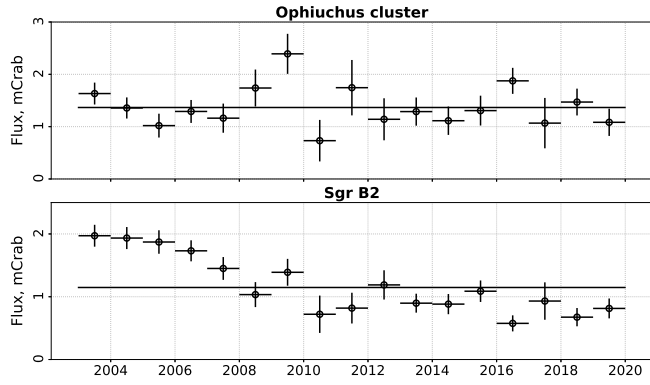


Figure 3. The light curves of the Ophiuchus cluster (upper plot) and Sgr B2 (bottom plot), obtained by *IBIS* in 2003–2019. Solid lines represent the best-fit constant functions for the Ophiuchus cluster and Sgr B2 light curves, shown in the upper and bottom plots, respectively.

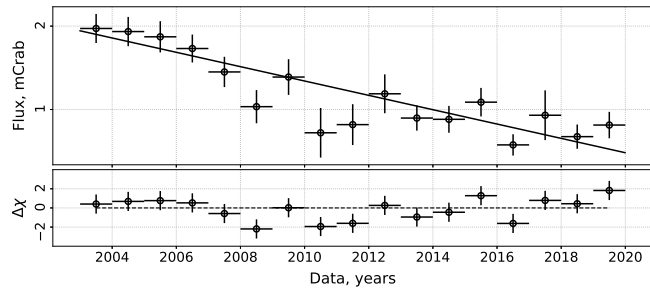


Figure 4. The light curve of Sgr B2 in the 30–80 keV energy band approximated with the linear function (upper plot) and residuals (bottom plot).

if present, is diluted within the one-year time bins, and on smaller time bins, the data quality does not allow us to draw any firm conclusions.

To describe the decreasing trend of the Sgr B2 emission with an additional background component, we applied a linear function of the form $A * T + B$, where A and B are coefficients in units of mCrab/yr and mCrab, correspondingly, and T is a time in years since 2003. This linear model provides a better fitting of the Sgr B2 light curve, as shown in Fig. 4 and listed in Table 1. To compare our results with that obtained by Terrier et al. (2010), we chose the time parameter $\tau_{1/2}$, a time of flux decrease by a factor of two from the flux initial value. Our estimation of $\tau_{1/2} = 12 \pm 2$ yrs obtained within the time interval of 2003–2020 is somewhat larger than $\tau_{1/2} = 8.2 \pm 1.7$ yrs determined by Terrier et al. (2010) in 2003–2009. The difference is probably caused by the longer fitting interval considered in the current work.

Then we suggested that there is a constant level in the Sgr B2 decreasing trend described by a linear piece-wise function in the following form:

$$F(T) = \begin{cases} A * T + B & \text{for } T \leq T_{\text{break}} \\ C & \text{for } T > T_{\text{break}} \end{cases}, \quad (1)$$

where T_{break} is a time when the Sgr B2 emission changes from a linear trend to a constant C level. The approximation of the light curve is shown in Fig. 5, with the best-fitting model parameters listed in Table 1. The piece-wise function describes the Sgr B2 light curve at better fit statistics compared to the constant and linear models. The characteristic time $\tau_{1/2} = 6 \pm 2$ yrs is in agreement with the Terrier et al. (2010) estimation within the uncertainties. Note that the constant level $C = 0.8 \pm 0.1$ mCrab measured after $T_{\text{break}} = 2011 \pm 3$

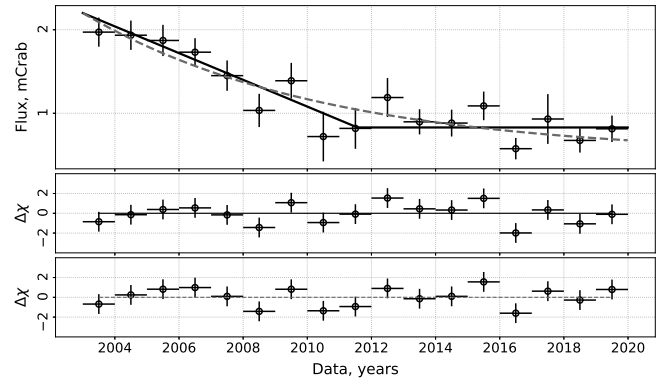


Figure 5. The 30–80 keV light curve of Sgr B2 approximated with the linear piece-wise and exponential functions, as shown in the upper plot, respectively, with solid and dashed lines, and the corresponding residuals are demonstrated in the middle and bottom panels.

Table 1. Best-fit parameters for the fitting procedure of the Sgr B2 light curve with the constant, linear, piece-wise, and exponential functions.

Parameter	Constant	Linear	Piece-wise	Exponential
A , mCrab/yr	—	-0.08 ± 0.01	-0.16 ± 0.06	—
B , mCrab	—	1.9 ± 0.14	2.2 ± 0.2	—
T_{break} , yrs	—	—	2011 ± 3	—
$\tau_{1/2}$, yrs	—	12 ± 2	6 ± 2	—
C , mCrab	~ 1.1	—	0.83 ± 0.1	$0.5^{+0.3}_{-0.6}$
F_0 , mCrab	—	—	—	$1.7^{+0.5}_{-0.3}$
τ , yrs	—	—	—	$7.5^{+7.1}_{-3.5}$
$\chi^2_{\text{red}}/d.o.f.$	7.4/16	1.48/15	1.09/14	1.04/14

is not consistent with zero flux background level, as it is expected for the coded-mask sky reconstruction method (see e.g., Krivonos et al. 2010, and references therein).

We divided the whole dataset from 2003 to 2019 into two time intervals T_1 and T_2 , separated by the year 2011 (orbit 1055), where a linear decay is replaced by a constant according to the linear piece-wise fit (Sect. 4). Fig. 6 demonstrates the T_1 and T_2 ficance maps in the 30–80 keV energy band. The Sgr B2 30–80 keV flux was measured at the level of 1.6 mCrab (23.5σ) and 0.8 mCrab (10.7σ), respectively, for the T_1 and T_2 datasets.

The Sgr B2 centroid positions at $RA=17^h47^m28^s.32$, $Dec.= -28^\circ21'10''.80$ and $RA=17^h47^m25^s.75$, $Dec.= -28^\circ25'08''.18$ measured during the T_1 and T_2 time intervals are shifted, respectively, by $2.3'$ and $2.7'$ from the position of the maximum column density of the cloud (Protheroe et al. 2008). The observed offsets are well consistent with the $3'$ localization uncertainty (2σ) for weak sources detected by *INTEGRAL/IBIS* (Krivonos et al. 2007).

Finally, we approximated the light curve of Sgr B2 by an exponential decay with a constant term C : $F_0 \times \exp^{-AT} + C$, where F_0 is an initial flux in mCrab units, τ is a lifetime expressed in the units of yrs. The best-fitting model describes the light curve at acceptable fit statistics $\chi^2_{\text{red}}/d.o.f. = 1.04/14$, as listed in Table 1 and shown in Fig. 5. The lifetime was estimated at $\tau = 7.5^{+7.1}_{-3.4}$ yrs, which is close to $\tau \sim 11$ yrs provided by Zhang et al. (2015) for the central $90''$ of Sgr B2.

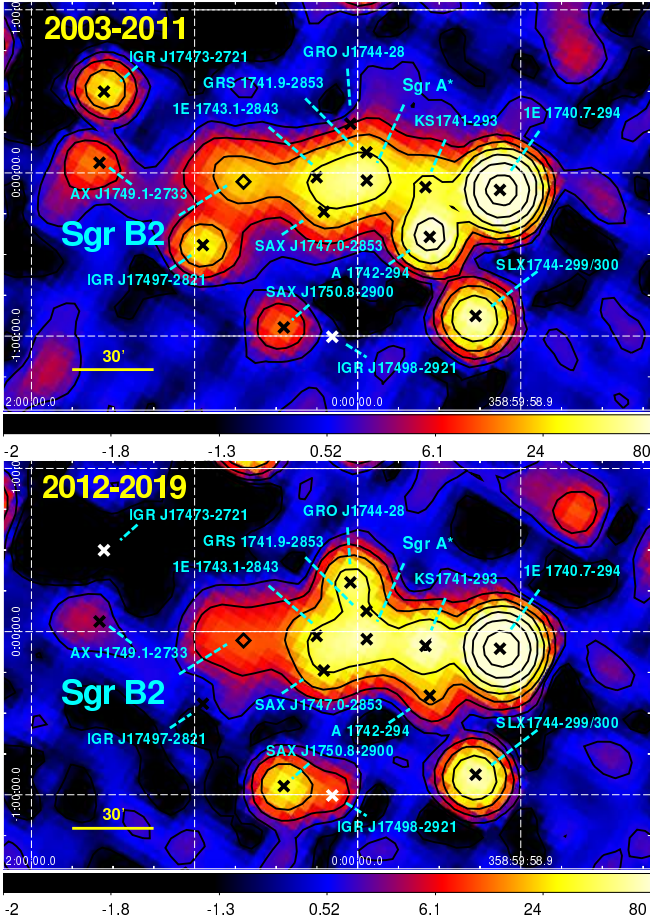


Figure 6. *IBIS* images of the GC region in the 30–80 keV energy band in detection significance units for the T1 and T2 time intervals are in the top and bottom panels, respectively. Contours and regions are the same as in Fig. 1.

5 SPECTRAL ANALYSIS

In this section, we analyse spectral information of Sgr B2 in the wide energy range 17–129 keV obtained for the T1 and T2 time intervals (Sect. 4). We extracted spectra from the sky images in different energy bands in the position of Sgr B2, as shown in Fig. 6. Note that the region of spectral extraction corresponds to the angular resolution of *IBIS/ISGRI* of $12'$. We excluded the first energy bin from the T2 spectrum due to the ongoing *ISGRI* detector degradation and loss of sensitivity at low energies (Caballero et al. 2013). Note that we also added a 5% systematic error in the spectral fitting procedures.

First, we tried to fit the obtained Sgr B2 region spectra (see Fig. 7) with a power-law model. For spectral fitting, we used the *xSPEC* package version 12.11.0 (Arnaud 1996), which is part of the *HEASOFT* v6.27 software. The results are listed in Table 2, where Γ is a photon index of the power-law model. For this and all following models, we calculated the 25–50 keV flux $F_{25-50 \text{ keV}}$ using the multiplicative model component *cflux* in *xSPEC*. The power-law model is in agreement only with the T2 spectrum (see Table 2), and its Γ is significantly greater than $\Gamma = 2.07 \pm 0.05$ obtained for the hard X-ray part of the broad-band analysis in Terrier et al. (2010). The upper plot in Fig. 8 shows the Sgr B2 region spectra fitted with the power-law model. Note that residuals of the T1 spectrum show evidence for a high-energy cutoff at ~ 40 keV.

Then we fitted both spectra using a power-law model with a high-energy cutoff. The best-fitting model parameters are listed in Table 2.

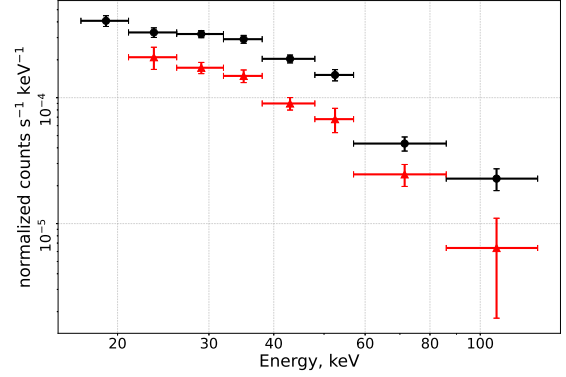


Figure 7. The Sgr B2 region spectra obtained in the 17–129 keV (black circles) and 21–129 keV (red triangles) energy band by *IBIS* during T1 (circles) and T2 (triangles).

The Sgr B2 region T1 spectrum is in good agreement with this model with a cutoff energy of $E_{\text{cut}} = 44^{+61}_{-18}$ keV (see bottom panel in Fig. 8). Due to the low quality of the T2 data, the photon index is not constrained by the fit, so we fixed it at the previously obtained value $\Gamma = 1.4$. We conclude that for the T1 spectrum, the cutoff power-law provides a better approximation than the simple power-law (see Table 2).

Assuming that the spectral shape has not changed from the T1 time interval to T2, we jointly fitted both spectra with the cutoff power-law model (see column Joint in Table 2). Here C_{cross} is a normalization constant of the T2 spectrum with respect to T1. The measured C_{cross} value of 0.51 ± 0.06 shows that the T1 flux has dropped by a factor of ~ 2 . The best-fit result has good statistics that indicate a possible similarity between the T1 and T2 spectral shapes.

Then we used the physically motivated *CREFL16* XSPEC table model (see description in Churazov et al. 2017), which describes a spectrum of a uniform gas cloud illuminated by an external source of a parallel X-ray emission beam. This model represents the reflected emission from the GC molecular clouds. The reflected emission depends on five parameters: a radial Thomson optical depth of the cloud τ_T , a slope of the primary power-law spectrum Γ , an abundance of heavy elements relative to Feldman (1992) Z/Z_{\odot} , a cosine of the viewing angle $\mu = \cos\Theta$, and a normalization. We fixed $\tau_T = 0.4$, $Z/Z_{\odot} = 1.9$ in accordance with Revnivtsev et al. (2004b) and considered the case in which Sgr B2 is in the same plane with Sgr A*, i.e., $\mu = \cos 90^\circ = 0$. (see Table 2). In this configuration, the *CREFL16* model well describes the T1 spectrum with $\Gamma = 2.30 \pm 0.13$. The T2 spectrum does not allow us to estimate Γ , so we fixed it at the T1 value assuming the same flare for both time intervals and obtained good fit statistics (see Table 2).

Alternatively to the reflection mechanism, the Sgr B2 X-ray emission may be caused by interaction of a molecular cloud material with cosmic ray particles. Tatischeff et al. (2012) studied a non-thermal emission of a neutral ambient medium caused by LECRe electrons and protons (hereafter LECRe and LECRp, respectively) and developed corresponding spectral models. We tested only the LECRp model due to the unphysical parameters of the LECRe model determined for the Sgr B2 emission by Zhang et al. (2015). The LECRp model depends on five parameters: a power-law slope of an accelerated cosmic ray (CR) spectrum s , a minimum energy of the CRs E_{min} , a metallicity of the ambient medium Z/Z_{\odot} , a path length of the CRs in the region Λ , a normalization of the model N_{LECRp} . We fixed $Z/Z_{\odot} = 2.5$,

Table 2. Best-fit parameters of different models after the fitting procedure of the Sgr B2 region spectra obtained in the T1 and T2 time intervals.

Parameters	T1	T2	Joint
Power-law			
Γ	~ 2.3	2.7 ± 0.3	—
$F_{25-50 \text{ keV}}^{\text{pow}}$ $10^{-12} \text{ erg cm}^{-2} \text{ s}^{-1}$	~ 13	7.2 ± 0.7	—
C_{cross}	—	—	—
$\chi_{\text{red}}^2/d.o.f.$	2.75/6	0.63/5	—
Cutoff power-law			
Γ	1.4 ± 0.6	1.4 (fixed)	$1.4^{+0.5}_{-0.6}$
E_{cut} , keV	44^{+61}_{-18}	35^{+12}_{-8}	43^{+48}_{-17}
$F_{25-50 \text{ keV}}^{\text{pow}}$ $10^{-12} \text{ erg cm}^{-2} \text{ s}^{-1}$	14 ± 1	$7.3^{+0.7}_{-0.8}$	13.9 ± 0.9
C_{cross}	—	—	0.51 ± 0.06
$\chi_{\text{red}}^2/d.o.f.$	1.51/5	0.55/5	1.08/11
<i>CREFL16</i>			
Γ	2.30 ± 0.13	2.3 (fixed)	2.35 ± 0.12
$F_{25-50 \text{ keV}}^{\text{pow}}$ $10^{-12} \text{ erg cm}^{-2} \text{ s}^{-1}$	13.6 ± 0.8	7.0 ± 0.7	13.6 ± 0.8
C_{cross}	—	—	0.52 ± 0.06
$\chi_{\text{red}}^2/d.o.f.$	1.53/6	0.85/6	1.14/12
<i>LECRp</i>			
Γ	—	2.7 ± 0.5	—
$N, 10^{-6} \text{ erg cm}^{-2} \text{ s}^{-1}$	—	$2.7^{+3.5}_{-1.3}$	—
$\chi_{\text{red}}^2/d.o.f.$	—	0.87/5	—

$\Lambda = 5 \times 10^{24} \text{ H-atoms cm}^{-2}$, $E_{\text{min}} = 10 \text{ MeV}$ in accordance with Zhang et al. (2015), while N_{LECRp} and s were free parameters. Due to the time variability in the Sgr B2 light curve at a few-year scale obtained for the T1 time interval (see Sect. 4), which contradicts the CR scenario (see e.g., Dogiel et al. 2014; Tatischeff et al. 2012), we applied this model only at the T2 spectrum. The obtained results are in Table 2.

6 DISCUSSION

The decreasing behavior of the Sgr B2 X-ray emission was observed with many X-ray telescopes (Inui et al. 2009; Terrier et al. 2010; Nobukawa et al. 2011; Zhang et al. 2015; Terrier et al. 2018). The most suitable hypothesis, explaining the time variability of the Sgr B2 hard X-ray emission, is the reflection of the SMBH Sgr A* X-ray flare. However, the question of how long the Sgr B2 emission will keep its decreasing trend and which mechanism will dominate the observed X-ray emission after the Sgr A* light front leaves the cloud remains open.

Previous observations of the Sgr B2 region by X-ray observatories *NuSTAR* and *XMM-Newton* showed that the Fe K_{α} flux of the central 90'' region in 2013 is consistent with the flux measured in 2012, but at the same time the 2013 flux is also consistent with the decreasing trend (Zhang et al. 2015). These authors concluded that if the Sgr B2 emission has reached its background level, *LECRp* may be the main contributor. Although if the Sgr B2 flux continues to decrease, the reflection scenario better describes the observed emission behaviour.

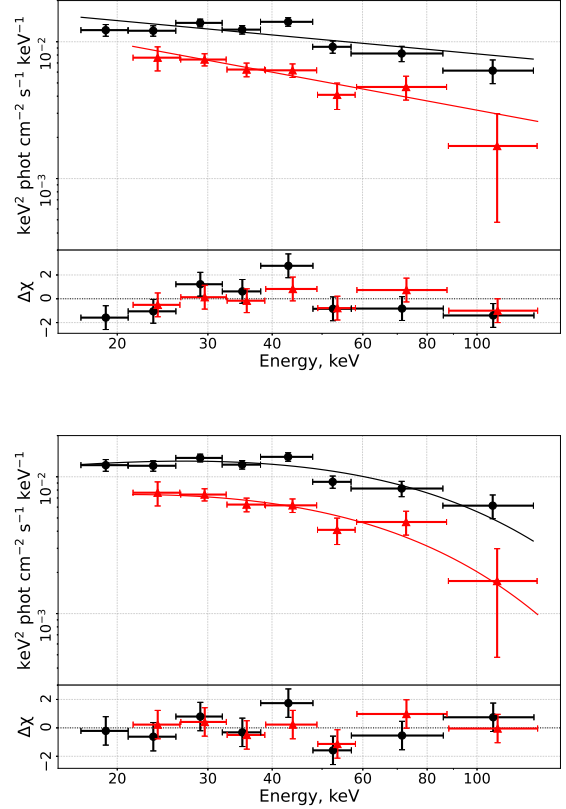


Figure 8. The Sgr B2 region spectra obtained in the 17–129 and 21–129 keV energy bands by *IBIS* during T1 (circles) and T2 (triangles), respectively. Black and red solid lines represent the best-fit simple power-law (top panel) and cutoff power-law (bottom panel) models for the Sgr B2 spectra obtained before and after T_{break} , respectively. For convenience, in Fig. 8, we do not present the complex models *CREFL16* and *LECRp*.

Also, Terrier et al. (2018) showed that in 2012 an extended X-ray emission from the Sgr B2 region was still detected with *XMM-Newton*.

A similar case was observed in a molecular cloud near the Arches stellar cluster in the GC. Both fluxes of the non-thermal continuum and the Fe K_{α} emission line demonstrate a decreasing trend with a similar timescale (Clavel et al. 2014; Krivonos et al. 2017a), however, also showing evidence for the constant emission level (Kuznetsova et al. 2019). Also, Chernyshov et al. (2018) considered two scenarios for the Arches cluster molecular cloud emission: two X-ray flares ~ 100 years and ~ 200 years ago, which were reflected from two different clouds located on the line-of-sight, and a combination of reflected emission and emission caused by the bombardment of the molecular cloud matter by cosmic rays. The first scenario strongly depends on the reflection geometry of two clouds and the iron abundances, while the second one is restricted by the photon index of the X-ray emission and needs the presence of a local cosmic ray particle accelerator. Also, note that the variability of the X-ray emission at different time scales of several years observed from other molecular clouds in the GC region (see e.g., Ponti et al. 2010, 2013; Clavel et al. 2013; Ryu et al. 2013; Churazov et al. 2017; Terrier et al. 2018) may be related to different light-crossing times and/or intrinsic flare durations.

The *INTEGRAL* observatory allows us to collect information about

the Sgr B2 region during the 17 years since 2003. Spatially consistent with Sgr B2, the hard X-ray source IGR1747 was detected during the considered time interval. The obtained 30–80 keV light curve of IGR1747 shows a linear decay, which changed to a constant level in 2011, that separated the time interval 2003–2020 into the T1 and T2 epochs. This result is in agreement with the assumption that the Sgr B2 flux in 2013 remains at the 2012 level (Zhang et al. 2015). Before 2011, the decay is characterized with $\tau_{1/2} = 6 \pm 2$ yrs that is consistent with the 2003–2009 *INTEGRAL* result $\tau_{1/2} = 8.2 \pm 1.7$ yrs (Terrier et al. 2010). Thus the *INTEGRAL* light curve supports the reflection scenario for the time interval before ~ 2011 . Assuming the dominating single scattering scenario over the whole studied period 2003–2020, characterized by a single linear trend, τ is estimated to be 12 ± 2 yrs. This value is slightly larger than that obtained by Terrier et al. (2010). It is worth noting that the decrease in the Sgr B2 hard X-ray continuum observed by *INTEGRAL* is in agreement with the overall drop of the 6.4 keV line flux measured by *XMM-Newton* in the same sky region (Rogers et al. 2021). This indicates that the Fe K_α line flux and the hard X-ray continuum are linked to each other, confirming the reflection scenario.

The spectral analysis also points to the reflection origin because the 17–129 keV spectrum agrees with the *CREFL16* model. The *INTEGRAL* T1 estimation of the initial flare slope $\Gamma = 2.30 \pm 0.13$ (at the 90% confidence interval) is in agreement with $\Gamma \sim 2$ obtained for the Sgr B2 90'' central region by *NuSTAR* (Ponti et al. 2010; Mori et al. 2015; Zhang et al. 2015). Also, Revnivtsev et al. (2004b) reported about the power-law with $\Gamma = 1.8 \pm 0.2$ (at the 1σ confidence interval) for the Sgr B2 spectrum using the *INTEGRAL* data collected in the 2003–2004 time interval. Furthermore, the similar slope $\Gamma \sim 2$ was estimated for other GC molecular clouds by the reflected emission (Mori et al. 2015; Krivonos et al. 2017a) and for the observed Sgr A* X-ray flares (Baganoff et al. 2001; Porquet et al. 2003, 2008; Nowak et al. 2012; Degenaar et al. 2013; Neilsen et al. 2013; Barrière et al. 2014; Zhang et al. 2017).

The LECR hypothesis can be rejected for this emission due to the Sgr B2 multi-year time variability. Point sources may be additional contributors to the T1 IGR1747 flux, but not the main ones because we did not detect any fast variability and the summed flux from the point sources did not describe all flux from the Sgr B2 region (see Sect. 6.3). Therefore, the reflection scenario is the most suitable for the Sgr B2 emission before 2011.

The main question is the origin of the observed constant emission after 2011 when the Sgr B2 flux dropped by a factor of ~ 2 and remained at this level until 2019. We did not detect any significant difference between the T1 (before 2011) and T2 (after 2011) spectral shapes of the Sgr B2 emission. Is the IGR1747 hard X-ray emission after 2011 still related to Sgr B2 molecular cloud or not?

6.1 Reflection scenario after 2011

Assuming that the light front from the Sgr A* flare has mostly left the cloud, another possible explanation of the observed remaining Sgr B2 emission is caused by a long-lived doubly-scattered albedo (Sunyaev & Churazov 1998; Odaka et al. 2011; Molaro et al. 2016), which probably became visible after 2011. The doubly-scattered albedo is expected to dominate single scatterings in hard X-rays due to a low photo-absorption and an additional enhancement by the down-scattering of high energy photons due to the Compton effect (Sazonov et al. 2020; Khabibullin et al. 2020).

6.2 Cosmic ray scenario

The constant T2 flux may be a sign of an interaction of the molecular cloud neutral matter with CRs. Zhang et al. (2015) suggested that in the case of the Fe K_α emission of the 90'' Sgr B2 region having reached its constant level in 2013, LECRp may be a major contributor. Zhang et al. (2015) rejected the LECRe hypothesis due to the unphysically large metallicity $Z/Z_\odot = 4.0^{+2.0}_{-0.6}$ and very low electron energy. The high value of the photon index $\Gamma = 2.7 \pm 0.3$ determined for the *INTEGRAL* T2 data obtained in the 21–129 keV energy band can be easily explained by the LECRp hypothesis, rather than the LECRe one (see Fig. 7 and 9 for the LECRp and Fig. 2 and 4 for the LECRe in Tatischeff et al. 2012). A good agreement between the *INTEGRAL* T2 spectrum and the LECRp model points to the possible LECRp nature of the T2 Sgr B2 region spectrum.

Assuming that Sgr B2 is in the plane of Sgr A*, i.e., at the $D = 8.178$ kpc distance (Gravity Collaboration et al. 2019), we estimated the power injected by the LECR 10 MeV – 1 GeV protons in the Sgr B2 region $dW/dt = 4\pi D^2 N_{\text{LECR}} = 2.1^{+2.6}_{-1.0} \times 10^{40}$ erg s⁻¹. This value is significantly greater (~ 10 times) than the *NuSTAR* estimation (Zhang et al. 2015), probably due to the larger *INTEGRAL* spectrum extraction region. Then, taking into account the uncertainties of E_{min} (see Sect. 5.2 in Tatischeff et al. 2012), we obtained $dW/dt = (4 - 90) \times 10^{39}$ erg s⁻¹. Note that the estimated slope of the CR source spectrum $s = 2.7 \pm 0.5$ is in contradiction with the slope $1.5 < s < 2$ predicted by the diffusive shock acceleration (DSA) theory, which was considered in Tatischeff et al. (2012). Therefore, we do not take into account the contribution from the suprathermal protons and possible heavier nuclei, and the estimation $dW/dt = (4 - 100) \times 10^{39}$ erg s⁻¹ is only a lower limit of the total CR power.

To investigate the ionization rate, we first determined the CR power deposited into the Sgr B2 cloud. The previously obtained LECRp power is $dW/dt \sim 2.1 \times 10^{40}$ erg s⁻¹. However the power deposited into the cloud is lower than the injected dW/dt due to two reasons: (1) the non-penetration into the cloud of the CRs with $E < E_{\text{min}}$ and (2) the escape from the cloud of the CRs with the highest energies (Tatischeff et al. 2012). Note that we considered only protons and did not do any corrections of the dW/dt related to the first reason because we are already taking into account only the CR particles with $E > E_{\text{min}}$. For $\Lambda = 5 \times 10^{24}$ H-atoms cm⁻², the protons with the energy $E > 180$ MeV are not stopped in the cloud (Tatischeff et al. 2012). Integrating the CR power taking into account only the CRs with $E > 10$ MeV/nucleon and $E < 180$ MeV/nucleon, we obtained that the power deposited by LECRs into the cloud is $\dot{W}_d \sim 1.9 \times 10^{40}$ erg s⁻¹ (90% of the dW/dt). Using the total mass of the Sgr B2 molecular cloud $M = 6 \times 10^6 M_\odot$ (Lis & Goldsmith 1990), we estimated the CR ionization rate at $\zeta_{\text{H}} \sim 5.6 \times 10^{-14}$ H⁻¹ s⁻¹ (see Equation 11 in Tatischeff et al. 2012). Such a CR ionization rate is too high compared with the GC CR ionization rate $\zeta_{\text{H}} \sim (1 - 3) \times 10^{-15}$ H⁻¹ s⁻¹ (Goto et al. 2011) and slightly higher than the Zhang et al. (2015) estimation $\zeta_{\text{H}} \sim (6 - 10) \times 10^{-15}$ H⁻¹ s⁻¹. Due to the high predicted CR ionization rate, we consider the LECRp scenario to be unfavorable.

Dogiel et al. (2011) predicted that in the case of the subrelativistic protons produced by accretion processes onto the SMBH Sgr A*, two X-ray emission components from the molecular cloud should be observed: a time variable reflected emission and a quasi-stationary emission caused by these protons. The authors predicted the time variations of the 6.4 keV Fe K_α equivalent width when the Sgr A* flare front passes through the Sgr B2 cloud and the reflected flux com-

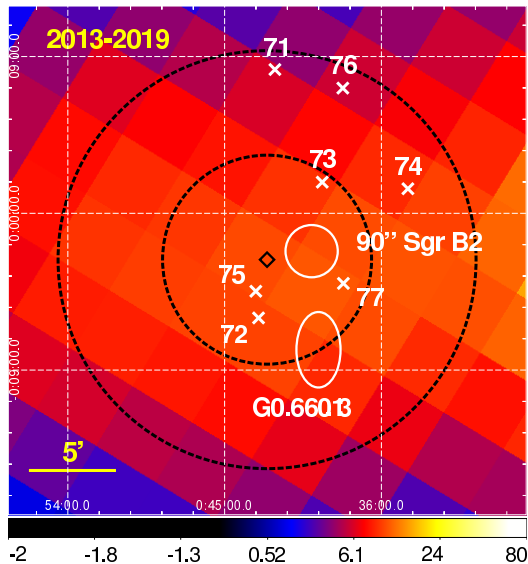


Figure 9. The close view of the T2 Sgr B2 image from Fig. 6. Black dashed circles with radii $R = 6 - 12'$ are centered at the *INTEGRAL* Sgr B2 position (diamond) obtained for the T2 data. Solid circle and ellipse are $R = 90''$ Sgr B2 region and G0.66–0.13 feature from (Zhang et al. 2015), respectively. Point sources reported in (Hong et al. 2016) are shown with crosses.

pletely drops. Future observations of Sgr B2 6.4 keV line emission will shed light on the nature of its emission.

6.3 Unresolved point sources scenario

The remaining Sgr B2 emission could also be explained by an integrated flux of the unresolved X-ray sources in this region. To check this, we sum up the fluxes from the known X-ray sources in the Sgr B2 region.

Zhang et al. (2015) presented the results of the *NuSTAR* observations of Sgr B2 with the coverage region almost matching the *INTEGRAL* region from which the IGR1747 emission was collected (a circle with radius equals *INTEGRAL FWHM* = $12'$). In this region, *NuSTAR* observed only three bright sources in the 10–40 keV energy band: the Sgr B2 core (circle region with $R = 90''$), the extended feature G0.66–0.13, and the point source CXOUGC J174652.9–282607 (see Fig. 1 in Zhang et al. 2015). We also considered point X-ray sources detected by *NuSTAR* during the hard X-ray survey of the GC region (see Table 5 in Hong et al. 2016) with maximum offset $11.4'$ from the T2 *INTEGRAL* Sgr B2 position (see Sect. 5). Fig. 9 demonstrates the *NuSTAR* source positions on the 30–80 keV *INTEGRAL* map. We recalculated the fluxes of each *NuSTAR* source in the *IBIS* energy band 25–50 keV and summed them to obtain the total flux $\sim 3.4 \times 10^{-12} \text{ erg cm}^{-2} \text{ s}^{-1}$ which turned out to be ~ 2 times lower than the flux $F_{25-50 \text{ keV}} = (7.2 \pm 0.7) \times 10^{-12} \text{ erg cm}^{-2} \text{ s}^{-1}$ measured by *INTEGRAL*. We conclude that the integrated flux from known X-ray sources does not account for more than half of the observed Sgr B2 emission after 2011.

7 SUMMARY

Thanks to the regular *INTEGRAL* observations of the GC region, we have a unique possibility to trace the long-term evolution of the Sgr B2 hard X-ray emission, broadly accepted as the X-ray reflected emission from the past flare activity of Sgr A*.

We constructed one-year averaged maps of the GC region observed by *INTEGRAL* in 2003–2020 that confirm fading of the hard X-ray emission. The sky maps after 2011 demonstrate a significant emission from the Sgr B2 position. We constructed the Sgr B2 light curve for the 2003–2019 time period and found that the light curve is better described with a piece-wise function than a linear one. The fitting procedure with the piece-wise function showed that in $2011 \pm 3 \text{ yr}$, there is a transition in the 30–80 keV Sgr B2 flux light curve from fading to constant. The existence of the break in the Sgr B2 time evolution may indicate a change in the emission generation mechanism. However, the possibility that the whole light curve is consistent with the linear decrease associated with the reflection scenario cannot be completely ruled out.

The spectral analysis showed that there is no difference in spectral shape before and after ~ 2011 . Both spectra are in good agreement with a power-law model with a high-energy cutoff at $\sim 43 \text{ keV}$. Also, both spectra support the reflection scenario of an X-ray flare with $\Gamma \sim 2.3$. The fading emission observed before 2011 is well explained by the reflection scenario, while the nature of the remaining emission is still unclear.

The low-energy CR protons model with primary power-law slope $s = 2.7 \pm 0.5$ describes the 2011–2019 spectrum well, but the estimated CR ionization rate $\zeta_{\text{H}} \sim 5.6 \times 10^{-14} \text{ H}^{-1} \text{ s}^{-1}$ is one order of magnitude higher than the GC value $\zeta_{\text{H}} \sim (1 - 3) \times 10^{-15} \text{ H}^{-1} \text{ s}^{-1}$ (Goto et al. 2011). Therefore this scenario is unfavorable for the emission observed after 2011. Part of this emission could be a result of the composition of unresolved point sources. The known *NuSTAR* sources could explain only about 50% of the observed *INTEGRAL* flux in 25–50 keV and do not dominate in the 2011–2019 Sgr B2 flux. Another significant part of the remaining Sgr B2 emission could be caused by multiple scatterings in the reflection scenario. Further observations are needed to precisely investigate the Sgr B2 region at low and high X-ray energies.

ACKNOWLEDGMENTS

This work is based on observations with *INTEGRAL*, an ESA project with instruments and the science data centre funded by ESA member states (especially the PI countries: Denmark, France, Germany, Italy, Switzerland, Spain), and Poland, and with the participation of Russia and the USA. We are grateful to Eugene Churazov, Ildar Khabibullin and Vincent Tatischeff for the useful comments and suggestions. E.K. and A.L. acknowledge support from the Russian Foundation for Basic Research (grant 19-32-90283). R.K. acknowledges support from the Russian Science Foundation (grant 19-12-00369). M.C. acknowledges financial support from the Centre National d’Etude Spatiales (CNES).

DATA AVAILABILITY

The *INTEGRAL* data underlying this article are publicly available at <http://www.isdc.unige.ch/>.

REFERENCES

- Arnaud K. A., 1996, in Jacoby G. H., Barnes J., eds, *Astronomical Society of the Pacific Conference Series Vol. 101, Astronomical Data Analysis Software and Systems V*. p. 17
- Baganoff F. K., et al., 2001, *Nature*, **413**, 45
- Baganoff F. K., et al., 2003, *ApJ*, **591**, 891

- Barrière N. M., et al., 2014, *ApJ*, **786**, 46
- Bélangier G., et al., 2006, *ApJ*, **636**, 275
- Caballero I., et al., 2013, arXiv e-prints, p. arXiv:1304.1349
- Chernyshov D. O., Ko C. M., Krivonos R. A., Dogiel V. A., Cheng K. S., 2018, *ApJ*, **863**, 85
- Chuard, D. et al., 2018, *A&A*, 610, A34
- Churazov E., et al., 2007, *A&A*, **467**, 529
- Churazov E., et al., 2014, *Nature*, **512**, 406
- Churazov E., Khabibullin I., Ponti G., Sunyaev R., 2017, *MNRAS*, **468**, 165
- Clavel M., Terrier R., Goldwurm A., Morris M. R., Ponti G., Soldi S., Trap G., 2013, *A&A*, **558**, A32
- Clavel M., Soldi S., Terrier R., Tatischeff V., Maurin G., Ponti G., Goldwurm A., Decourchelle A., 2014, *MNRAS*, **443**, L129
- Degenaar N., Miller J. M., Kennea J., Gehrels N., Reynolds M. T., Wijnands R., 2013, *ApJ*, **769**, 155
- Dogiel V. A., et al., 2009, *PASJ*, **61**, 1093
- Dogiel V., Chernyshov D., Koyama K., Nobukawa M., Cheng K.-S., 2011, *PASJ*, **63**, 535
- Dogiel V. A., Chernyshov D. O., Tatischeff V., Cheng K.-S., Terrier R., 2013, *The Astrophysical Journal*, **771**, L43
- Dogiel V., Chernyshov D., Kiselev A., Cheng K.-S., 2014, *Astroparticle Physics*, **54**, 33
- Feldman U., 1992, *Phys. Scr.*, **46**, 202
- Goto M., Usuda T., Geballe T. R., Indriolo N., McCall B. J., Henning T., Oka T., 2011, *PASJ*, **63**, L13
- Gravity Collaboration et al., 2019, *A&A*, **625**, L10
- Hong J., et al., 2016, *ApJ*, **825**, 132
- Inui T., Koyama K., Matsumoto H., Tsuru T. G., 2009, *PASJ*, **61**, S241
- Khabibullin I., Churazov E., Sunyaev R., Federrath C., Seifried D., Walch S., 2020, *MNRAS*, **495**, 1414
- Koyama K., Maeda Y., Sonobe T., Takeshima T., Tanaka Y., Yamauchi S., 1996, *PASJ*, **48**, 249
- Krivonos R., Revnivtsev M., Lutovinov A., Sazonov S., Churazov E., Sunyaev R., 2007, *A&A*, **475**, 775
- Krivonos R., Revnivtsev M., Tsygankov S., Sazonov S., Vikhlinin A., Pavlinsky M., Churazov E., Sunyaev R., 2010, *A&A*, **519**, A107
- Krivonos R., Tsygankov S., Lutovinov A., Revnivtsev M., Churazov E., Sunyaev R., 2012, *A&A*, **545**, A27
- Krivonos R. A., et al., 2014, *ApJ*, **781**, 107
- Krivonos R., et al., 2017a, *MNRAS*, **468**, 2822
- Krivonos R. A., Tsygankov S. S., Mereminskiy I. A., Lutovinov A. A., Sazonov S. Y., Sunyaev R. A., 2017b, *MNRAS*, **470**, 512
- Kuznetsova E., et al., 2019, *MNRAS*, **484**, 1627
- Lebrun F., et al., 2003, *A&A*, **411**, L141
- Lis D. C., Goldsmith P. F., 1990, *ApJ*, **356**, 195
- Madsen K. K., Forster K., Grefenstette B. W., Harrison F. A., Stern D., 2017, *ApJ*, **841**, 56
- Molaro M., Khatri R., Sunyaev R. A., 2016, *A&A*, **589**, A88
- Mori K., et al., 2015, *ApJ*, **814**, 94
- Morris M., Serabyn E., 1996, *ARA&A*, **34**, 645
- Neilsen J., et al., 2013, *ApJ*, **774**, 42
- Nobukawa M., Ryu S. G., Tsuru T. G., Koyama K., 2011, *ApJ*, **739**, L52
- Nowak M. A., et al., 2012, *ApJ*, **759**, 95
- Odaka H., Aharonian F., Watanabe S., Tanaka Y., Khangulyan D., Takahashi T., 2011, *ApJ*, **740**, 103
- Oh K., et al., 2018, *ApJS*, **235**, 4
- Ponti G., Terrier R., Goldwurm A., Bélangier G., Trap G., 2010, *ApJ*, **714**, 732
- Ponti G., Morris M. R., Terrier R., Goldwurm A., 2013, in Torres D. F., Reimer O., eds, Vol. 34, *Cosmic Rays in Star-Forming Environments*. p. 331 (arXiv:1210.3034), doi:10.1007/978-3-642-35410-6_26
- Porquet D., Predehl P., Aschenbach B., Grosso N., Goldwurm A., Gondoni P., Warwick R. S., Decourchelle A., 2003, *A&A*, **407**, L17
- Porquet D., et al., 2008, *A&A*, **488**, 549
- Protheroe R. J., Ott J., Ekers R. D., Jones D. I., Crocker R. M., 2008, *MNRAS*, **390**, 683
- Reid M. J., Menten K. M., Zheng X. W., Brunthaler A., Xu Y., 2009, *ApJ*, **705**, 1548
- Revnivtsev M. G., et al., 2004a, *Astronomy Letters*, **30**, 382
- Revnivtsev M. G., et al., 2004b, *A&A*, **425**, L49
- Rogers F., Zhang S., Perez K., Clavel M., Taylor A., 2021, arXiv e-prints, p. arXiv:2108.13399
- Ryu S. G., Nobukawa M., Nakashima S., Tsuru T. G., Koyama K., Uchiyama H., 2013, *Publications of the Astronomical Society of Japan*, **65**
- Sazonov S., et al., 2020, *New Astron. Rev.*, **88**, 101536
- Sunyaev R., Churazov E., 1998, *MNRAS*, **297**, 1279
- Sunyaev R. A., Markevitch M., Pavlinsky M., 1993, *ApJ*, **407**, 606
- Tatischeff V., 2003, in Motch C., Hameury J.-M., eds, *EAS Publications Series* Vol. 7, *EAS Publications Series*. p. 79 (arXiv:astro-ph/0208397), doi:10.1051/eas:2003038
- Tatischeff V., Decourchelle A., Maurin G., 2012, *A&A*, **546**, A88
- Terrier R., et al., 2010, *ApJ*, **719**, 143
- Terrier R., Clavel M., Soldi S., Goldwurm A., Ponti G., Morris M. R., Chuard D., 2018, *A&A*, **612**, A102
- Ubertini P., et al., 2003, *A&A*, **411**, L131
- Walls M., Chernyakova M., Terrier R., Goldwurm A., 2016, *Monthly Notices of the Royal Astronomical Society*, **463**, 2893
- Winkler C., et al., 2003, *A&A*, **411**, L1
- Zhang S., et al., 2015, *ApJ*, **815**, 132
- Zhang S., et al., 2017, *ApJ*, **843**, 96

This paper has been typeset from a $\text{\TeX}/\text{\LaTeX}$ file prepared by the author.